Structural Design of Safety Steel Device of Railway Vehicles Through Analytical and Experimental Investigations

Jovan Tanaskovic[1], Francis Franklin[2], Nenad Radovic[3], Fatima Zivic[4]

[1]University of Belgrade Faculty of Mechanical Engineering, Kraljice Marije 16, 11000 Belgrade, Serbia, jtanaskovic@mas.bg.ac.rs

[2]School of Engineering, Newcastle University, Newcastle upon Tyne NE1 7RU, United Kingdom, francis.franklin@ncl.ac.uk

[3]University of Belgrade Faculty of Technology and Metallurgy, Karnegijeva 4, 11000 Belgrade, Serbia, nenrad@tmf.bg.ac.rs

[4]University of Kragujevac Faculty of Engineering, Sestre Janjic 6, Kragujevac 34000, Serbia, zivic@kg.ac.rs

Abstract: The subject of this paper is the structural design of a safety steel device that is located between the standard wagon buffer and the collision energy absorber. The safety steel device is a sacrifical part able to withstand normal operating loads from the buffer across the absorber to the vehicle bearing structure without any permanent deformation, but experiences fully controlled fracture when the load exceeds the defined threshold. Following fracture, the load path is through the energy absorber. The sacrificial part is a ring made from quenched and tempered low alloyed steel with precisely defined heat treatment and material properties. Experimental investigations of scaled samples were performed to get mechanical characteristics of the material and geometry. A full-scale prototype of the safety device was produced, and final quasi-static and dynamic experiments were conducted. The results validate the anaytical predictions, and thus validate the design method used here for dimensioning the safety steel device.

Keywords: Safety Steel Device; Controlled Fracture; Analytical Dimensioning; Experimental Investigations

1 Introduction

Development and design of standard elements of railway vehicles present a classical job for an experienced designer or researcher. When it comes to design of special parts that are installed in the current bearing structure, especially if those parts have

a role to controll fracture at the exactly defined load, the design is more challenging. Such sacrificial parts are often included in passive safety elements and have a direct impact on the safety, primarily passengers but also vehicles and railway infrastructure. To maximise reliability and safety, research must focus on the right choice of grade of material and shape of geometry as well as the most appropriate way of controlled deformation. Deformation must be absolutely controlled, and it is necessary to analyse in detail loads and requirements defined in standards for the strength of railway vehicles [1, 2].

There are many different ways to connect active and passive safety elements (for controlled activation of energy absorbers) in the railway vehicles structure [3-5]. The anti-climb device and energy absorber are parts of the passive safety assembly and one method for connecting these is based on the process of cutting the outer surface of the wall of steel and aluminium tubes. The impact of cutting depth, the geometry of dies, and stroke of cutting were analysed by experimental investigations in the quasi-static and dynamic behaviour. Experimental results showed that the cutting deformation mode is more stable for aluminium tube and that longitudinal cutting force is correspondingly larger for harder materials and larger cutting depths. Including a shrinking tube energy absorber in the process of collision kinetic energy absorption is one more way for the connection of active and passive absorption elements, and this was analysed by Moreno et al. [6]. This paper describes the shrinking process of energy absorption and imperfection that may arise during deformation. During normal exploitation, an automatic coupler absorbs forces through the elastic device without the need for activation of passive safety elements. At the moment of collision, contact forces increase rapidly and leading to activation of passive safety elements installed behind the anti-climbing device. The authors developed and validated a numerical model also that can be used for additional analyses. Absorption characteristics of square cross-section tube that use the folding process for energy absorption have been analysed [7]. Initial force is determined as the critical value of force that causes local buckling of the tube. These passive elements are also installed behind the anti-climb system and take the role of energy absorption when the contact forces exceed normal exploitation values. Results of experimental and numerical investigations of shrinking, folding, curling, splitting, combined tube collision energy absorbers, and sliding friction and wear are discussed in Refs [8-14]. Next to the requests defined in the standard, the condition of the rail track has a significant role in dynamic stability as well as railway safety in general [15, 16]. A new idea for connection of active and passive safety elements is presented here. A safety device consisting of a sacrificial element to control the load path, joins the standard buffer and tube absorber, Fig. 1. The role of it is to transfer normal exploitation loads from standard buffer to the wagon bearing structure by passing the absorber and preventing therefore undesired any permanent deformation. Exceeding normal exploitation loads, in the case of collision, leads to controlled fracture of safety device at the exactly defined shearing area, and to activation of the tube absorber. This paper in detail describes analytically dimensioning of safety device and experimental validation of defined

dimensions and material properties. A developed analytical model can be used for further dimensioning this type of safety device as well as similar devices which are a part of collision energy absorber or for some other purpose that requires controlled fracture.

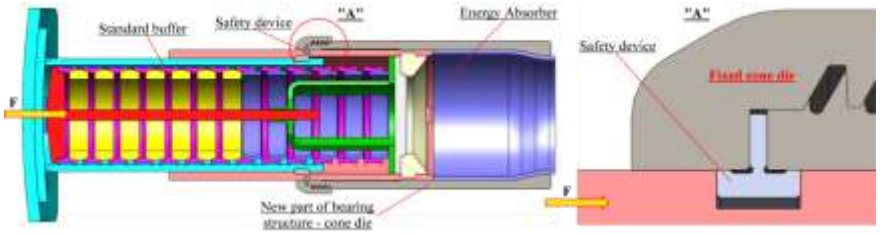

Figure 1
Working principle of safety device

2 Material Characterisation and Proof Design

The geometry and dimensioning of the safety device is critically dependent on the material properties. Material characterization combined analytical determination of critical load using scaled samples with experimental investigations on scaled samples, leading to the final analytical determination of dimensions of the cross-section of a full-scale model of a prototype safety device.

2.1 Preliminary Analytical Design of Safety Device

Safety steel device has a role to transfer normal exploitation loads from the standard buffing elements, bypassing the absorption element, to the vehicle bearing structure, and to break in controlled manner if exploitation loads exceed limit values. The structure of standard buffing elements and the implementation of an energy absorber in line with it requires that the safety device breaks through a clean shearing process. To achieve a controlled break, normal operating stresses need to be below the yield point, which needs to be clearly defined, and ideally below the fatigue limit also, so that there is no failure or plastic deformation of the sacrificial component. The threshold load for activation of the energy damper should be sufficient to exceed the yield stress or the fracture stress. Since the strength, as a crucial design parameter, depends on material composition and quality, heat treatment and to some extent geometry, a scaled model of the safety device was prepared to check performance against values of tensile strength defined in the standards [17].

The geometry and function of the safety device led to the choice of quench and tempered low alloyed steel in grade 42CrMo4 for production. This grade of steel has guaranteed chemical composition while the desired values of mechanical

properties can be obtained by adequate heat treatment. Two different values of hardness were analysed, 42 and 52 HRC, as well as two different cross-sections of safety device, Fig. 2.

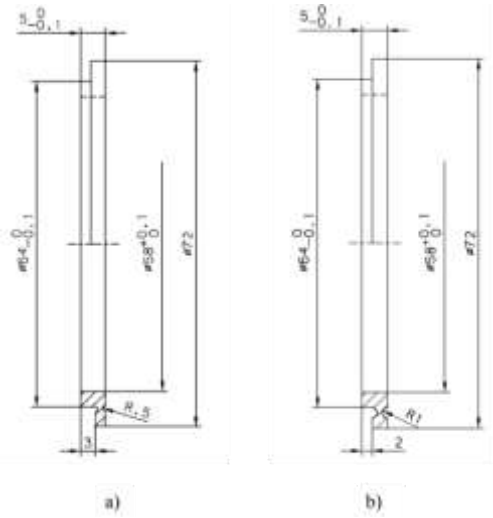

Figure 2
Dimensions of scaled safety devices: a) initial radius at shearing area 0.5 mm, b) initial radius at shearing area 1.0 mm

Values of tensile strength σ_M, for hardness 42 HRC and 52 HRC, are ≈1330 MPa and ≈1800 MPa respectively [18-20]. The estimated breaking force is calculated in Table 1, where the ratio (s_f) of limiting shear stress to limiting tensile stress was determined in Ref. [21], and the standard formula for maximum shear stress (VQ/Ib) is used for bending of a rectangular section. Based purely on shear area calculations, therefore, the expected values of breaking force, for two different values of hardness 42 HRC and 52 HRC, are approximately 231 kN and 312 kN respectively. These can be regarded as upper limits, however, with lower limits provided by the bending calculation, i.e., 154 kN and 208 kN respectively. A threshold is set for activation of the energy absorber just above the upper limit.

2.2 Experimental Investigation of the Safety Device

In accordance with the dimensions, defined in Fig. 2, scaled samples were prepared as well as supporting testing tool, Fig. 3a. Samples were made from quench and tempered low alloyed steel in grade 42CrMo4. Three samples were prepared and passed heat treatments. Two samples, manufactured in accordance to dimensions showed in Fig. 2a and Fig. 2b, after heat treatment have a hardness of 42 HRC. One sample was manufactured in accordance to dimensions showed in Fig. 2a with hardness of 52 HRC after heat treatment. Preliminary experimental investigations

were performed on the electro-mechanical testing machine at Institute GOSA that has a maximum load of 250 kN, Fig. 3b. Following experimental investigations, the microstructure of the fractured samples was studied and discussed.

Figure 3

Sample and testing machine: a) Sample of safety device and support tool: 1 - Safety device, 2 – Base of support tool, 3 – Safety nut and 4 – Bushing with circular groove; b) Electro-mechanical testing machine: 1 – Sample ready for test; 2 – Machine head

Table 1

Estimation of breaking force using simple shear and bending shear stress calculations

Geometry			
Thickness of shearing cross-section	b	1	mm
Diameter at shearing cross-section	D_s	65	mm
Area of shearing cross-section = $\pi D_s b$	A_s	204	mm^2
2nd Moment of area of shearing cross-section (treated as rectangular section) = $\pi D_s b^3 / 12$	I_s	17	mm^4
Common Factors			
Ratio of limiting shear stress to limiting tensile stress i.e., τ_M / σ_M	s_f	0.85	
Ratio of limiting stress to activation stress (τ_M / τ_r)	s	0.98	
Grade 42CrMo4: Hardness 42 HRC			
Tensile strength	σ_M	1330	MPa
Limiting shear stress = $s_f \sigma_M$	τ_M	1130	MPa
Critical load (simple shear) = $\tau_M A_s$	F_s	231	kN
Critical load (maximum shear stress from bending) $F_b = F_s / 1.5$	F_b	154	kN
Activation load = F_s / s	F_a	236	kN
Grade 42CrMo4: Hardness 52 HRC			
Tensile strength [18-20]	σ_M	1800	MPa
Limiting shear stress = $s_f \sigma_M$	τ_M	1530	MPa
Critical load (simple shear) = $\tau_M A_s$	F_s	312	kN
Critical load (maximum shear stress from bending) $F_b = F_s / 1.5$	F_b	208	kN
Activation load = F_s / s	F_a	319	kN

2.3 Experimental Results

During experiments on the scaled samples, deformation resistance was measured. Recorded load-displacement curves showing the breaking force are shown in Fig. 4a-c.

Experimental and analytical values of breaking force are presented in Table 2. Values of deformation resistance and tensile strength obtained by the experimental test are a close match to the lower limit obtained by analytical calculation. This indicates that bending stresses are critical, which are not included in the shear area calculation. The similarity of results in Fig. 4a and 4b indicates that the difference in notch radius is not hugely significant; as would be expected, the larger notch radius corresponds to a high failure load, but further testing and analysis would be needed to verify this.

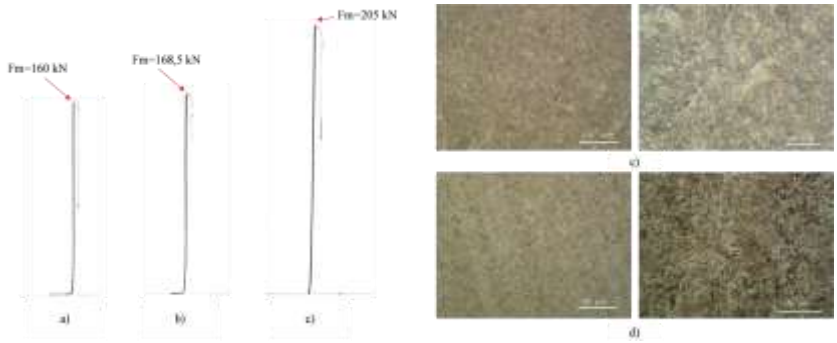

Figure 4

Diagram of breaking force F_m: a) 42 HRC, Fig. 2a; b) 42 HRC, Fig. 2b; c) 52 HRC, Fig. 2a; and Microstructure of braked safety device: c) hardness 42 HRC; d) hardness - 52 HRC

Table 2

Experimental and analytical values of breaking force

	42HRC		52HRC	
	F_M [kN]	σ_M [MPa]	F_M [kN]	σ_M [MPa]
Analytical values	154 – 231	1330	208 – 312	1800
Experimental values	160 – 168.5	783	205	1004

2.4 Microstructure of Tested Scaled Safety Device

The microstructure of the shearing area was studied using microscope Neofit 30. Fig. 4c,d show the microstructure of the fractured scaled samples.

Both hardness grades show material structures characteristic of typical tempered martensite. After quenching, obtained martensitic microstructure was subjected to tempering. During tempering, chromium based carbides are formed. Depending on tempering temperature, different rate of carbide nucleation and growth of carbides

can be obtained, providing variation in size of particles, as shown in Fig. 4c,d. Therefore, due to variation of carbide size, resistance to deformation is not the same, providing difference in mechanical properties [22, 23].

Based on this, including experimental results and the position of the safety device in the assembly, and the need to function during normal exploitation as well as during collision, hardness 42 HRC is chosen for the safety device. The lower value of hardness is more acceptable for a dynamically loaded design element because a higher value leads to an increase in brittleness and a decrease in toughness.

3 Experimental Research

After analysis of preliminary design and results obtained by tests of scaled safety device, the final design of safety device was prepared and checked via following tests: a) quasi-static test on the hydraulic press and b) dynamic test via collision of two passenger wagons on the industrial railway track at GOSA Rolling Stock Company.

3.1 Determination of Final Design Dimensions

To match the standard buffer, the full scale device requires a shear diameter of 220 mm (compared to 65 mm for the scale device) and a target activation load of 800 kN. Column A in Table 3 indicates that for Grade 42CrMo4 (42 HRC) a thickness of 1.5 mm is appropriate for the shearing cross-section.

Fig. 5a shows the main dimensions of the safety device cross-section. The geometry of the cross-section has been redesigned to provide a clean shear, i.e., breaking of safety device. Manufacture of the safety device is straightforward, but requires high precision. Fig. 5b shows the prototype of a safety device prepared for experimental investigations. After machining by scraping and realised final heat treatment, the safety device cut in two equal parts for assembling in the absorber assembly.

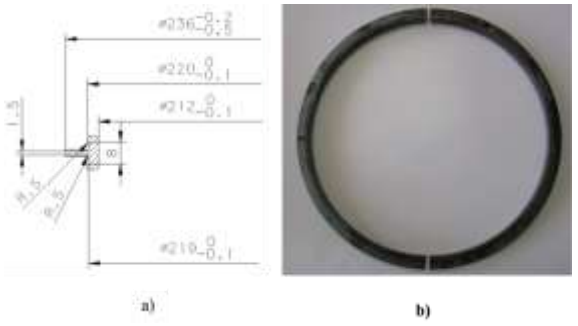

Figure 5
Final design of safety device: a) Dimensions of full scaled safety device; b) Prototype

Table 3

Estimation of breaking force for full scale device with target activation load 800 kN. A: Initial estimate. B: Ratio s adjusted to match experimental results. C: Adjusted thickness to match target.

Geometry		**A**	**B**	**C**	
Thickness of shearing cross-section	b	1.5	1.5	**1.7**	mm
Diameter at shearing cross-section	D_s	220	220	220	mm
Area of shearing cross-section = $\pi D_s b$	A_s	1037	1037	1175	mm^2
2nd Moment of area of shearing cross-section (treated as rectangular section) = $\pi D_s b^3 / 12$	I_s	194	194	283	mm^4
Common Factors					
Ratio of limiting shear stress to limiting tensile stress i.e., τ_M / σ_M	s_f	0.85	0.85	0.85	
Ratio of limiting stress to activation stress (τ_M / τ_r)	s	0.98	**1.11**	1.11	
Grade 42CrMo4: Hardness 42 HRC					
Tensile strength [18-20]	σ_M	1330	1330	1330	MPa
Limiting shear stress = $s_f \sigma_M$	τ_M	1130	1130	1130	MPa
Critical load (simple shear) = $\tau_M A_s$	F_s	1172	1172	1328	kN
Critical load (maximum shear stress from bending) $F_b = F_s / 1.5$	F_b	781	781	886	kN
Activation load (bending) = F_b / s	F_a	797	704	798	kN

3.2 Experimental Investigations

The goal of experimental investigations was to check defined geometry of safety device under exactly defined loads as well as the way of deformation of it. Safety device has a role to join standard buffer and absorber and to transfer normal exploitation loads without any permanent deformation. When loads exceed the exactly defined value, comes to controlled break of safety device and absorber starts to work. The following tests were performed: a) quasi-static test on the hydraulic press LITOSTROJ 2500 kN and b) dynamic "crash" test on the open railway track at GOSA Rolling Stock Company, Fig. 6.

During the quasi-static test, reaction force was measured at defined speed of machine head of 50 mm/s. The dynamic test was realized with a wagon speed of 3.4 m/s, while the reaction force and displacement were measured. To get requested way of deformation of safety device, i.e. clean shear, a special tool shown in Fig. 6c was used.

Figure 6
Experimental investigations of prototype: a) Quasi-static test; b) Dynamic - Crash test; c) Test assembly

3.2.1 Results of Experimental Investigations

Figs. 7 and 8 show results obtained by experimental investigations, through force vs. time and force vs. displacement diagrams. Two samples in quasi-static behaviour were tested. Very close values of breaking forces of 824 kN and 843 kN were measured, Fig. 7. Both curves show brittle fracture of safety devices.

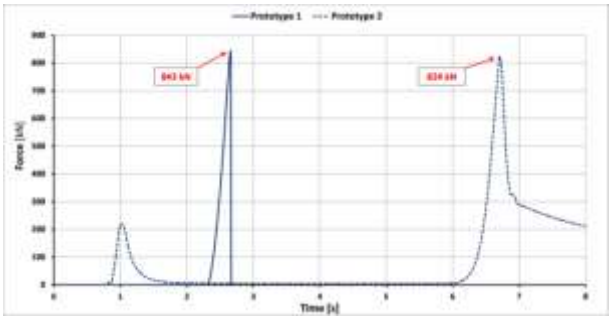

Figure 7
Breaking force of safety device - Quasi-static test

A full collision test of two passenger wagons gave force vs. displacement diagrams that characterize three zones, Fig. 8: the first zone presents work of standard buffer; the second zone presents fracture of safety device and the third zone presents work of absorber. Brittle fracture of safety device can be seen in these diagrams as well. Values of fracture forces measured during the dynamic test are 705 kN and 816 kN, respectively.

Fig. 8b,c shows look of safety device before and after fracture. It can be seen clearly that the safety device is fractured at an exactly designed place (shearing area of width 1.5 mm).

The safety device is designed to transfer a load up to 800 kN without plastic deformation. This means that the normal exploitation load under this value is acceptable and will not lead to the fracture of the safety device.

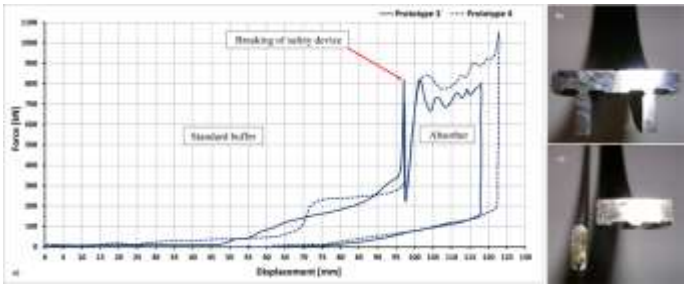

Figure 8
Breaking force of safety device: a) Dynamic crash test, b) Cross section before fracture, c) Cross section after fracture

Results obtained by experimental investigations shown values of fracture force that are slightly higher than 800 kN, which confirms the stability of the safety device and validates the analytical determination of cross-section dimensions of the safety device. The exception represents the fracture force value obtained by the dynamic test of 705 kN, which is assumed to be the related to the imperfection of production and inevitable asymmetry of collision contacts. The maximal deviation of the value of fracture force of the safety device is about 5%, which is acceptable and confirms the dimensioning analytical method as appropriate for further dimensioning of different types of safety device as well as similar devices.

The consistency of results across quasi-static and dynamic tests suggests strain rate-dependent effects can be neglected. This is very important from the aspect of working principles of safety devices and dynamic behaviour in exploitation. However, if the outlier result of 705 kN is representative, this would correspond to a lower activation stress and a value of $s = 1.11$ in the calculation (Column B in Table 3). To prevent premature activation, a thicker cross-section width of 1.7 mm would be advisable (Column C in Table 3).

There are further questions that need to be addressed in future research, in particular the fatigue response of the safety devices to normal operating loads, and the likelihood of crack initiation at the free ends of the split ring.

Conclusions

The development of the passive safety elements is a very challenging and complex job that requires precise design and manufacture, careful choice of materials and properties, as well as mounting in a new or current bearing wagon structure. One of the most important design steps is the correct design of the connection between active and passive elements. This paper has presented in detail the design of a sacrificial component that has a role to be fractured at a defined load and thus to redirect the load path away from the energy absorber until an impact event.

The precise fracture requires careful choice of material and heat treatment to control mechanical properties. Calculation and testing during the design process are

necessary to get reliable parameters for dimensioning of elements. Experimental results show that values of tensile strength of quench and tempered low alloyed steel in grade 42CrMo4 obtained by standard tensile tests and experimental tests of scaled samples of safety device have a close match to bending failure predictions.

A full-scale safety device was designed and tested in quasi-static and dynamic experimental investigations. Generally close and consistent results indicate strain-rate dependence is not a major factor, which suggests sufficiently ductile material, despite evidence of brittle fracture. Some further research is necessary to determine suitable safety factors and to study fatigue response in normal operation, but the experimental results presented here provide partial validation of the design methodology for the proposed safety device.

Acknowledgement

This work was supported by the Ministry of Education, Science and Technological Development of Republic of Serbia, Project No. 451-03-9/2021-14/200105 and 451-03-9/2021-14/200107.

References

[1] EN 15227:2008; Railway applications - Crashworthiness requirements for railway vehicle body

[2] EN 12663-1:2015; Railway applications - Structural requirements of railway vehicle bodies - Part 1: Locomotives and passenger rolling stock (and alternative method for freight wagons)

[3] Guangjun G., Weiyuan G., Jian L., Haipeng D., Xiang Z., Wei C., Experimental investigation of an active–passive integration energy absorber for railway vehicles, Thin-Walled Structures, Vol. 117, pp. 89-97, 2017

[4] Weiyuan G., Guangjun G., Jian L., Yao Y., Crushing analysis and multi-objective optimization of a cutting aluminium tube absorber for railway vehicles under quasi-static loading, Thin-Walled Structures, Vol. 123, pp. 395-408, 2018

[5] Junyan W., Zhaijun L., Mu Z., Tianjun W., Chengming S., Haihong L., Coupled thermal–structural analysis and multi-objective optimization of a cutting-type energy-absorbing structure for subway vehicles, Thin-Walled Structures, Vol. 141, pp. 360-373, 2019

[6] Moreno C., Winnett J., Williams T., On the effect of anisotropy on the performance and simulation of shrinking tubes used as energy absorbers for railway vehicles, Thin-Walled Structures, Vol. 161, https://doi.org/10.1016/j.tws.2021.107513, 2021

[7] Jian L.,Guangjun G., Haipeng D., Crushing analysis and multi-objective optimization of a railway vehicle driver's cab, Thin-Walled Structures, Vol. 107, pp. 554-563, 2016

[8] Tanasković J., Milković D. Lučanin V., Miloradović N., Experimental and numerical analysis of the characteristics of combined collision energy absorber, Facta Universitatis, Series: Mechanical Engineering, Vol. 10, No. 2, pp. 125-136, 2012

[9] Hosseini A., Hosseini Tehrani P., Study on new crashworthy buffers in railway, International Journal of Railway Research, Vol. 1, No. 2, pp. 59-73, 2014

[10] Tanaskovic J., Milkovic D., Lucanin V., Vasic Franklin G., Experimental investigations of the shrinking–splitting tube collision energy absorber, Thin-Walled Structures, Vol. 86, pp. 142-147, 2015

[11] Tanasković J., Franklin F., Dišić A., Mišković Ž., Numerical validation of the combined extrusion-splitting process of energy absorption through experimental study, Exp Tech, Vol. 41, pp. 421-431, 2017

[12] Tanasković J., Franklin F., Mitrović A., Dišić A., Experimental research of absorption properties of rigid foam filled circular seamless tube energy absorber under quasi-static axial load, Proc IMechE Part F: J Rail and Rapid Transit, http://dx.doi.org/10.1177/0954409720976034

[13] Harouz R., Lakehal A., Khelil K., Dedry O., Hashemi N., Boudebane S., Dry siliding friction and wear of the WC/TIC-CO in contact with Al_2O_3 for two sliding speeds, Facta Universitatis, Series: Mechanical Engineering, 2020, https://doi.org/10.22190/FUME200310039H

[14] Shilko V. E., Grigoriev S. A., Yu. Smolin Yu. A., A descrete element formalism for modelling wear particle formation in contact between sliding metals, Facta Universitatis, Series: Mechanical Engineering, Vol. 19, No. 1, pp. 7-22, 2021

[15] A. Németh, S. Fischer, Investigation of the glued insulated rail joints applied to CWR track, Facta Universitatis, Series: Mechanical Engineering, 2021, doi: 10.22190/FUME210331040N

[16] M. Sysyn, O. Nabochenko, V. Kovalchuk, M. Przybyłowicz, S. Fischer, Investigation of interlocking effect of crushed stone ballast during dynamic loading. Reports in Mechanical Engineering, Vol. 2, No. 1, pp. 65-76, 2021, https://doi.org/10.31181/rme200102065s

[17] DIN EN 10083-3:2007; Steels for quenching and tempering – Part 3: Technical delivery conditions for alloy steels

[18] Kraut B., Mechanical engineering manual, Technical book, Croatia, Zagreb, 1976 (in Serbian-Croatian)

[19] EN 10132-3:2000; Cold rolled narrow steel strip for heat treatment – Technical delivery conditions - Part 3: Steels for quenching and tempering

[20] Szala M., Winiarski G., Wójcik L., Bulzak T., Effect of Annealing Time and Temperature Parameters on the Microstructure, Hardness, and Strain-

Hardening Coefficients of 42CrMo4 Steel, Materials, 13(9), 2022, http://dx.doi.org/10.3390/ma13092022

[21] Veriga S., Mechanical elements 1 - First book General part, University of Belgrade Faculty of Mechanical Engineering, Belgrade, 1990

[22] Smallman R. E., Bishop J., Modern Physical Metallurgy and Materials Engineering, Science, process, applications, Sixth Edition Butterworth-Heinemann, Oxford, 1999

[23] Dieter G. E. Mechanical Metallurgy. SI Metric Edition, Mc Graw-Hill Book Co., New York, 1988